EARTH SURFACE PROCESSES AND LANDFORMS
Earth Surf. Process. Landforms (2014)

Published online in Wiley Online Library
(wileyonlinelibrary.com) DOI: 10.1002/esp.3550

Robust classification for the joint velocity-intermittency structure of turbulent flow over fixed and mobile bedforms

Christopher J. Keylock,[1]* Arvind Singh,[2] Jeremy G. Venditti[3] and Efi Foufoula-Georgiou[2]
[1] Sheffield Fluid Mechanics Group and Department of Civil and Structural Engineering, University of Sheffield, Sheffield, UK
[2] Department of Civil Engineering, St Anthony Falls Laboratory, and National Center for Earth-Surface Dynamics, University of Minnesota, Minneapolis, MN, USA
[3] Department of Geography, Simon Fraser University, Burnaby, British Columbia, Canada

Received 11 November 2013; Revised 28 January 2014; Accepted 10 February 2014

*Correspondence to: Christopher J. Keylock, Sheffield Fluid Mechanics Group and Department of Civil and Structural Engineering, University of Sheffield, Mappin Street, Sheffield S1 3JD, UK. E-mail: c.keylock@sheffield.ac.uk

ESPL
Earth Surface Processes and Landforms

ABSTRACT: Two datasets of turbulence velocities collected over different bedform types under contrasting experimental conditions show similarity in terms of velocity-intermittency characteristics and suggest a universality to the velocity-intermittency structure for flow over bedforms. One dataset was obtained by sampling flow over static bedforms in different locations, and the other was based on a static position but mobile bedforms. A flow classification based on the velocity-intermittency behaviour is shown to reveal some differences from that based on an analysis of Reynolds stresses, boundary layer correlation and turbulent kinetic energy. This may be attributed to the intermittency variable, which captures the local effect of individual turbulent flow structures. Locations in the wake region or the outer layer of the flow are both shown to have a velocity-intermittency behaviour that departs from that for idealized wakes or outer layer flow because of the superposition of localized flow structures generated by bedforms. The combined effect of this yields a velocity-intermittency structure unique to bedform flow.

The use of a time series of a single velocity component highlights the potential power of our approach for field, numerical and laboratory studies. The further validation of the velocity-intermittency method for non-idealized flows undertaken here suggests that this technique can be used for flow classification purposes in geomorphology, hydraulics, meteorology and environmental fluid mechanics. © 2014 The Authors. Earth Surface Processes and Landforms published by John Wiley & Sons Ltd.

KEYWORDS: bedforms; turbulence; velocity-intermittency structure; quadrants

Introduction

The unique and non-classical nature of environmental turbulence is an important reason why so many geomorphic processes have proven to be complex. For example, flow over gravel beds has been shown to depart from a classical boundary layer owing to the presence of macroturbulent structures (Shvidchenko and Pender, 2001; Roy *et al.*, 2004; Hardy *et al.*, 2007) and, in both aeolian and fluvial environments, the flow exhibits a complex interaction with bedforms on a variety of scales (Dinehart, 1992; Walker and Nickling, 2002; Best, 2005; Franklin and Charru, 2011; Singh *et al.*, 2011; Omidyeganeh and Piomelli, 2013a). An important first step for making progress in this area is to be able to identify the characteristics of environmental turbulence successfully and consistently. Ideally, this should be based on methods that can be readily applied in the field. This typically means data should be in the form of a velocity times series rather than based on spatial fields of the type obtained from particle imaging velocimetry (PIV) (Lelouvetel *et al.*, 2009; Hardy *et al.*, 2011) or numerical modelling (Chang *et al.*, 2011). Hence techniques based on invariants of the velocity gradient stress tensor (Dubief and Delcayre, 2000; Chakraborty *et al.*, 2005) or on characterizing the spatial evolution of flow structures using finite-size Lyapunov exponents (Haller, 2001) are not readily applicable.

Recently, it has been proposed that the joint velocity-intermittency structure of the flow, as determined from a time series of the longitudinal velocity component, can be used for classifying turbulence and for providing an insight into the physics of non-classical turbulent flows (Keylock *et al.*, 2012c). Intermittency is indicative of the passage of coherent structures, resulting in localized departures from classical, Kolmogorov-type turbulence even in the inertial regime (Kolmogorov, 1941; Frisch *et al.*, 1978; Dowker and Ohkitani, 2012). Standard measures derived from single-point measurements (turbulent kinetic energy, Reynolds stresses) do not contain this information directly. Furthermore, and from a

morefundamental perspective, Kolmogorov assumed in his derivation of the scaling laws for velocity fluctuations in turbulence that the velocity and intermittency were independent. While Keylock *et al.* (2012c) were able to show that this was a reasonable approximation for homogeneous, isotropic turbulence (HIT) – the conditions Kolmogorov assumed – it was clearly not the case for other flows. Hence it is argued that, to understand energy transfers near geomorphic boundaries, where HIT is a very poor assumption, fluvial geomorphologists need to take more explicit account of the non-classical nature of turbulence in these regions. Our technique provides both a means to do this and one that is amenable to field, laboratory or numerical investigation.

In particular, this study concerns the turbulence characteristics of flow over mobile and fixed bedforms. A great deal of the complexity in understanding the geomorphology and sedimentology of these phenomena is a consequence of the complex coupling between bedform morphology, sediment transport and turbulence processes. This is in no small part due to the importance of the flow structures that are generated (Best, 2005; Omidyeganeh and Piomelli, 2013b). Typically, field studies on bedform flow dynamics are undertaken over mobile bedforms, whereas laboratory and numerical research fix the bedforms in place. Thus it is important to compare the results from these different reference frames. Venditti and Bauer (2005) compared the flow structure measured over a mobile dune in the Green River with data obtained from the flow field behind fixed dunes in the laboratory. Similarities existed for a range of variables including Reynolds stresses, turbulence intensity and the correlation between velocity components. Furthermore, the oscillations in the wake region collapsed with the Strouhal number (frequency non-dimensionalized by a length and velocity scale) for the field and laboratory data. This work suggested that there are strong commonalities between the two cases, but no work has yet investigated whether the velocity-intermittency structure is also similar for these two cases. We test this hypothesis in this study for the first time.

If similarities are found, they provide further confirmation that the velocity-intermittency method developed by Keylock *et al.* (2012c) is robust and is a useful tool for classifying the flow structure in geomorphologically relevant situations. Not only does this open up the possibility for a range of studies examining this characteristic of environmental turbulence for very different boundary conditions (aeolian or fluvial flows through vegetation, for example), but it also provides a means for more readily comparing measurements made in the laboratory, where coherent structures might have been identified using PIV or similar, to field data consisting of velocity time series from a single point.

Velocity-intermittency structure

Results presented by Keylock *et al.* (2012c) showed that it was possible to discriminate between various flows by their velocity-intermittency structure. As explained more fully in the Methods section, this technique is based on forming quadrants constructed in the domain of the longitudinal velocity fluctuations and the corresponding fluctuating pointwise Hölder exponents. Considering that small Hölder exponents represent the presence of local discontinuities, while a large positive exponent indicates smoothness, the four resulting quadrants represent, relative to the mean conditions, fast–smooth flow (Q1), slow–smooth (Q2), slow–rough (Q3) and fast–rough (Q4) flow. By observing the proportional occupancy of each quadrant (i.e. its relative 'fullness'), one can quantify the predominant velocity-intermittency structure of the velocity series. By introducing a threshold condition, H, traditionally termed a 'hole size' in the quadrant literature, one can focus on the more extreme cases (large absolute values for the joint velocity and Hölder exponent fluctuations). Hence one can plot the percentage of points in each quadrant as a function of H (normalizing each time by the total number of points exceeding H). Such a plot is shown in Figure 1; a constant line at 25% would represent an equal presence of all quadrant conditions irrespective of H. This is what one would expect for idealized, homogeneous and isotropic turbulence (Kolmogorov, 1941) and is indeed what one finds from analysing such data (Keylock *et al.*, 2012c). However, the data in Figure 1 clearly depart from this idealized case, highlighting some of the complexity of environmental turbulence (lack of isotropy, non-equilibrium flow, etc.).

The data in Figure 1 are the results for flow over mobile bedforms (Keylock *et al.*, 2013), a turbulent jet (Renner *et al.*,

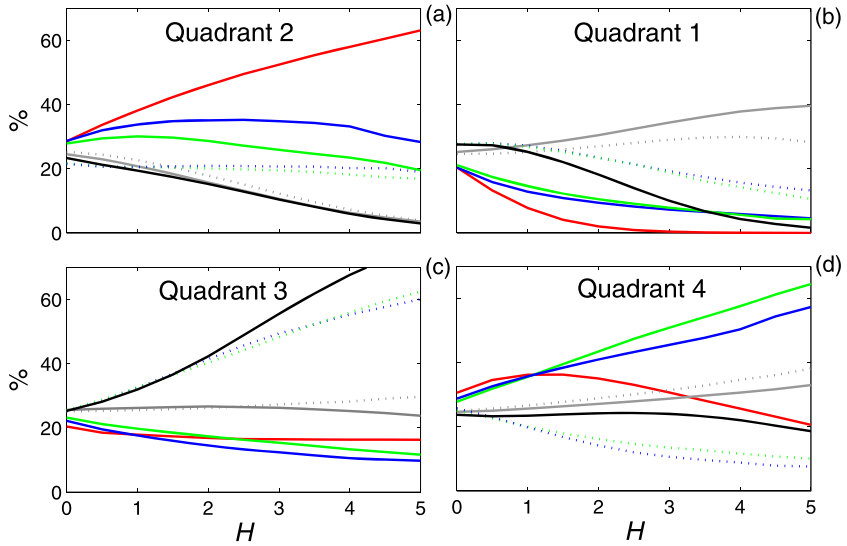

Figure 1. Analysis of velocity-intermittency-based quadrants. Results for flow over mobile gravel bedforms are shown as a solid black line. Additional lines are for a turbulent jet (red), wake data at 8.5 ms^{-1} (grey dotted) and 24.3 ms^{-1} (grey), and data near the wall (solid lines) and higher into the flow (dotted lines) at 6 ms^{-1} (blue) and 8 ms^{-1} (green) for a rough wall boundary layer. This figure is taken from Keylock CJ, Singh A, Foufoula-Georgiou E. 2013. The influence of bedforms on the velocity-intermittency structure of turbulent flow over a gravel bed, *Geophysical Research Letters* **40**: 1–5, doi:10.1002/grl.50337 (copyright American Geophysical Union) and is reproduced with the permission of the AGU.

2001), wake flows at two Reynolds numbers (Stresing *et al.*, 2010), as well as for a rough wall boundary layer at different heights from the wall (less than 20 mm or approximately 150 wall units and greater than 120 mm or ~ 700 wall units), and for two Reynolds numbers (Keylock *et al.*, 2012b). The flow over bedforms (black line) exhibits a general similarity to outer boundary layer flow (dotted green and blue lines). However, there is an excess contribution in quadrant 4 for the bedform data, which corresponds to the periods where the probe is affected by upstream shear generation (Keylock *et al.*, 2013). Because the velocity-intermittency characteristics of these data differ from the more classical flows examined in Figure 1, throughout the rest of this study we classify velocity-intermittency characteristics that resemble this case as 'bedform flow'. There is a clear difference in the behaviour of the outer layer and the bedform flow compared to the jet (rising trend in quadrant 2), wake data (rising trend in quadrant 1) and near-wall flow (rising trend in quadrant 4). That these cases appear so different is why we believe that this new technique is an effective tool for flow classification.

In addition to the high-frequency (at least 5000 Hz) and long-duration (thousands of integral timescales) fluid mechanics datasets, Keylock *et al.* (2012c) applied this method successfully with much shorter-duration and lower-frequency acoustic Doppler velocimeter (ADV) data where measurements were acquired for 5 min at 25 Hz, equating to about 150 integral scales. The integral scale was evaluated from the amplitude weighted mean frequency of the Fourier amplitude spectrum (Mazzi and Vassilicos, 2004). These latter time series were obtained in a region of complex dynamics – the near wall flow over a rough, fixed gravel bed, immediately downstream of a parallel-channel confluence and further evidence for the robustness of these data with respect to numerical modelling results and statistical convergence, is provided in Keylock *et al.* (2014). The results were encouraging: sites positioned far from the region of vortex impingement on the bed (either laterally or significantly downstreamof this region) exhibited a similar pattern to each other, while those close to vortex impingement were also grouped together. All sites exhibited the general characteristics seen in the benchmark data for a near-wall boundary layer dataset.

Aims of this study

The first goal of this paper is to test the flow classification scheme of Keylock *et al.* (2012c) against two datasets collected for flow over bedforms: one over low-amplitude gravel bedforms, and one over larger-amplitude, artificial bedforms, which were manufactured to be smooth. In the former case the bed is mobile, while in the latter the bed is fixed. The Keylock *et al.* (2013) data were collected over migrating gravel bedforms at one elevation and the Venditti and Bennett (2000) data were collected over a grid that covered the whole bedform field along the centre line of the channel. A consistent classification of the flow provides further confidence in the velocity-intermittency quadrant technique developed by Keylock *et al.* (2012c) and demonstrates for the first time that results are insensitive to the frame of reference adopted (what might be termed 'bedform Eulerian' or 'bedform Lagrangian' data collection). Furthermore, universality in the velocity-intermittency structure can be utilized in the future for deriving turbulence closures for numerical simulations of flow over geomorphological boundaries that capture the novel velocity-intermittency behaviour of such flows, which is of potential significance for modelling sediment entrainment and transport processes correctly.

The second goal is to use the results from the velocity-intermittency coupling to make inferences about the flow characteristics and to compare these to results obtained using more conventional flow variables. In particular, we make use of a study of the Reynolds stress, boundary layer correlation and turbulence production by Venditti and Bennett (2000). We are able to show that a study of velocity-intermittency coupling complements such analyses by providing specific information on the nature of turbulent flow structures. In particular, as a unique bedform flow type was identified using this method by Keylock *et al.* (2013), we are able to re-characterize regions of the flow domain that, based on conventional variables, exhibit wake or outer layer characteristics, as having a velocity-intermittency structure that clearly exhibits the imprint of bedform-generated turbulence. Thus we are able to refine traditional classifications of flow turbulence in geomorphic, near-wall flows.

Methods

Given a time series for the longitudinal velocity component, $u_1(t)$, we make use of a Reynolds decomposition to isolate the fluctuating velocity, $u_1'(t) = u_1(t) - < u_1 >$, where the angle brackets indicate a mean value and the prime indicates the fluctuating term. To simplify notation, we commonly drop an explicit recognition of the time dependence of the fluctuating terms in much of what follows. Classic quadrant analysis then utilizes u_1' together with the fluctuating vertical component, u_3', to produce a flow classification based on the signs of these terms (Lu and Willmarth, 1973). Quadrant analysis has been applied extensively in field, laboratory, theoretical and numerical studies in geomorphology and hydraulics (Nakagawa and Nezu, 1977; Nelson *et al.*, 1995; Fernandez *et al.*, 2006; Chapman *et al.*, 2012). In this paper we refer to each of these quadrants by their name rather than number to avoid confusion with what follows: outward interactions $\left(u_1' > 0, u_3' > 0\right)$; ejections $\left(u_1' < 0, u_3' > 0\right)$; inward interactions $\left(u_1' < 0, u_3' < 0\right)$; and sweeps $\left(u_1' > 0, u_3' < 0\right)$.

Our velocity-intermittency classification scheme is inspired by this framework. However, u_3' is replaced by the Hölder series for u_1'. This notion is intimately related to concepts of fractality and multifractality, which are widely employed in geomorphic investigations (Klinkenberg and Goodchild, 1992; Butler *et al.*, 2001; Posadas *et al.*, 2003; Singh *et al.*, 2011). While the fractal dimension provides a measure of the average scaling behaviour of variations in a signal, departures from this average are often detected, both in geomorphic forms (Gagnon *et al.*, 2003) and in processes. In the latter case, a Brownian motion that respects the classic Kolmogorov view of inertial range turbulence (Kolmogorov, 1941) with a slope of the energy spectrum of $-(2 - <\alpha>) = -5/3$, where $<\alpha> = 1/3$ is the average Hölder exponent, is a well-known instance of a fractal process. However, the passage of flow structures results in departures from homogeneous fractality, giving rise to corrections, for which various forms have been postulated (Kolmogorov, 1962; Frisch *et al.*, 1978; Dowker and Ohkitani, 2012). These introduce a degree of multifractality (Meneveau and Sreenivasan, 1991), and the techniques used to characterize this essentially aim to estimate the histogram of Hölder exponents (Muzy *et al.*, 1991). This is a complex problem for finitely sampled data and is typically handled by using wavelet methods and a Legendre transform. Owing to the importance of multifractality in geophysical data series, Schertzer and Lovejoy (1987) proposed the Universal Multifractal Formalism as a framework for summarizing the multifractal nature of geophysical data series. The first exponent is the average Hölder exponent, $<\alpha>$, while the second is a measure of variation

about $<\alpha>$. The third is a measure of the distribution function from which the data are sampled. Note that by studying all $\alpha(t)$ we have more information than is contained in these three summary statistics.

Computing the time series of Hölder exponents (a Hölder series, $\alpha(t)$) rather than summary statistics such as the mean, $<\alpha>$, and standard deviation, $\sigma(\alpha)$, is not trivial. However, methods have been proposed to do this (Kolwankar and Lévy Véhel, 2002; Seuret and Lévy Véhel, 2003) and testing by Keylock (2010) showed that the variance scaling approach (Kolwankar and Lévy Véhel, 2002) could replicate the observed behaviour of multifractional Brownian motions with good accuracy. Consequently, we adopted that method here. As departures from $<\alpha>$ indicate the passage of flow structures, there is a logic to using $\alpha(t)$ for extracting energetic flow periods from turbulence datasets (Keylock, 2008, 2009).

More formally, the Hölder series $\alpha_1(t)$, of $u_1(t)$, is defined as

$$|u_1(t) - u_1(t+\tau)| \sim C|\tau|^{\alpha_1(t)} \tag{1}$$

where C is a constant and τ is a displacement in time (see Venugopal *et al.*, 2006, for a review). The mean of $\alpha_1(t)$, $<\alpha_1>$, can be viewed as the Hurst exponent (Hurst, 1951) for the time series. Note that when the velocity signal is locally rougher, the pointwise Hölder exponent, $\alpha_1(t)$, will be smaller, reflecting a higher local value of the local fractal dimension, D_f. Because $u_1(t)$ and $\alpha_1(t)$ are measured in different units, we standardize the fluctuating values by their respective standard deviations σ:

$$\begin{aligned} u_1'*(t) &= u_1'(t)/\sigma(u_1) \\ \alpha_1'*(t) &= \alpha_1'(t)/\sigma(\alpha_1) \end{aligned} \tag{2}$$

Hence we may formulate quadrants based on the changes in sign of $u_1'*$ and $\alpha_1'*$: Q1 $\left(u_1'*>0, \alpha_1'*>0\right)$; Q2 $\left(u_1'*<0, \alpha_1'*>0\right)$; Q3 $\left(u_1'*<0, \alpha_1'*<0\right)$; and, Q4 $\left(u_1'*>0, \alpha_1'*<0\right)$. These may be interpreted, qualitatively, as follows: fast flow-low turbulence (Q1); slow flow-low turbulence (Q2); slow flow-high turbulence (Q3); and, fast flow-high turbulence (Q4).

The final step to our analysis introduces a threshold hole size, H, defined in terms of the standard deviations of the two variables (in a manner that is broadly similar to convention (Bogard and Tiederman, 1986), except that we have already normalized each variable by its standard deviation to handle their difference in dimensions). Thus a threshold exceedance is deemed to exist when

$$\left|u_1'*(t)\alpha_1'*(t)\right| \geq H \tag{3}$$

rather than $\left|u_1'(t)u_3'(t)\right| \geq \sigma(u_1)\sigma(u_1)H$. We then record the proportion of the time that the flow occupies each quadrant as a function of H. For each value of H we renormalize the percentages to sum to 100%. Thus an analysis at $H=0$ intrinsically involves 100% of the data. By $H=2$, we may only be looking at 5% of the dataset, but our percentages still sum to 100%. While some studies using traditional quadrant analysis then group consecutive occurrences in the same quadrant into flow events and examine the statistics of these events, we do not do this here.

Experimental Data

The data from this study are from two sources. The primary dataset consists of 28 velocity time series obtained for 120 s with an ADV at 25 Hz for a flow over fixed, two-dimensional dunes (Venditti and Bennett, 2000). The experiment was conducted at the National Sedimentation Laboratory, US Department of Agriculture, in Oxford, Mississippi. A tilting and recirculating flume 15.2 m long, 1 m wide and 0.25 m deep was used in the study. Twenty-four two-dimensional steel dunes 0.6 m long and 0.04 m high (each with a slip face angle of 30°) were fixed to the floor of the flume. The Froude number adopted was 0.35, with a mean flow velocity of 0.458 m s^{-1}, a maximum flow depth of $D=0.19$ m, and a mean discharge of 0.079 m^3 s^{-1}. An attempt was made to produce an equilibrium flow by adjusting the slope until the same flow depth occurred (± 2 mm) over five successive dune crests in the measurement section of the flume. This gave a mean water surface slopeof 0.00181. The ADV data were collected at the locations shown in Figure 2 and were filtered with a Gaussian low-pass filter (half-power frequency of 12.5 Hz) (Biron *et al.*, 1995). Further details on this experimental design and the measurement details are provided in Venditti and Bennett (2000) and Venditti and Bauer (2005).

The second set is the high-frequency (200 Hz), long-duration (5 h) $u_1(t)$ time series measured over a mobile gravel bed

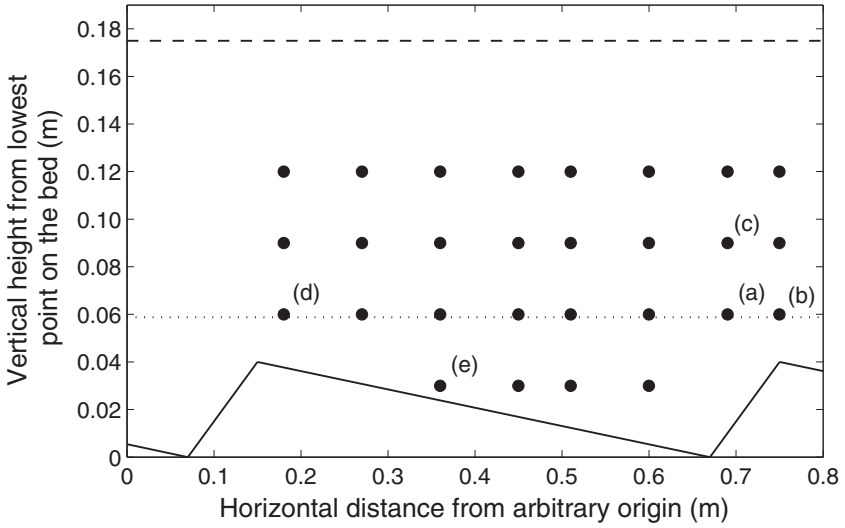

Figure 2. The 28 flow measurement locations used by Venditti and Bennett (2000) shown with a black circle. The dunes are shown with a solid line, the maximum water surface elevation with a dashed line, and the average height of the probe above the mean bed elevation in the experimental set-up of Singh *et al.* (2010) is given by a dotted line. The labels identify sites used in Figure 3.

surface with an ADV studied in Keylock *et al*. (2013). Simultaneous bed elevation data were recorded at 0.2 Hz using sonic transducers. The data were obtained from an experiment in the 84 m long, 2.7 m wide main channel facility at St Anthony Falls Laboratory, University of Minnesota. The flume is of a partial-recirculating type (the sediment may recirculate while the water flows through the flume without recirculation). The channel has a 55 m long test section with a poorly sorted gravel bed. The gravel used in these experiments had a $D_{50} = 11.3$ mm and was mixed with sand ($D_{50} = 1$ mm) in a ratio of 85:15. Experiments were conducted with the bed in a dynamic equilibrium state (evaluated by determining the stability of the 60 min average sediment flux at the downstream end of the working section). The ADV was positioned in the centreline of the flume approximately 0.15 m above the mean bed elevation at ~ 25% of the flow depth. As shown by the dotted line in Figure 2, this corresponds well to the 0.06 m ($z/D = 0.316$) row of ADV positions employed by Venditti and Bennett (2000). Further details on this experimental design and the measurement details are provided in Singh *et al*. (2009, 2010). A summary of the relevant experimental information for the two experiments is provided in Table I.

Results

Velocity-intermittency structure at selected sites

Figure 3 shows two occupancy-H plots constructed in a similar fashion to Figure 1. The upper panels compare the results for the flow determined by Keylock *et al*. (2013) (in red) with that found at a similar height in the Venditti and Bennett (2000) data ($z = 0.06$ m) at two locations furthest from shear processes generated at the crest ($x = 0.69$ m and 0.75 m). These are shown as positions (a) and (b) in Figure 2. There is very little difference between these data, indicating that similar flow processes are operating. The lower panel plots data from three other locations for illustrative purposes. Location (c) is higher into the flow ($x = 0.69$ m, $z = 0.09$ m) and is qualitatively similar to the results from Keylock *et al*. (2013), but with a stronger decrease of occupancy in Q2 and a stronger rise in Q3. The other two sites show differences in that the slopes in a given quadrant are not necessarily the same as for the Keylock *et al*. (2013) data. In particular, the flow at position (d) (squares) exhibits a rise in Q1 and position (e) a rise in Q4 and a lack of decay in Q2. An inspection of Figure 2 shows that these points are close to the dune crest and the closest to the lower boundary, respectively. Hence, some differences in spatial flow characteristics exist and these are explained below.

Table I. Summary information on the two experiments considered in this study. The value in parentheses is the ratio of the bedform advection velocity to the mean flow velocity)

	Venditti and Bennett (2000)	Singh *et al*. (2011)
Max. flow depth (m)	0.19	0.55
Mean flow velocity (m s $^{-1}$)	0.458	1.18
Bedform advection velocity (m s $^{-1}$)	0	3.9×10^{-3} (3.3×10^{-3})
Mean sediment diameter (mm)	0	7.7
Froude number	0.35	0.51

Velocity-intermittency structure at all sites

We can summarize our results effectively by approximating the lines seen in Figure 1 or 3 with a straight line and then recording the slopes in each quadrant. Our results for all 28 positions are shown in Figure 4. It is clear that the majority of sites, away from boundaries, exhibit a clear positive slope in Q3, in agreement with the results for flow over bedforms in Figure 1. At $z = 0.06$ m, which more closely corresponds to the elevation for the bedform flow type results in Figure 1, Q3 is not as dominant on average, but, of the eight plots at this height, all exhibit a positive slope for Q3 and in six cases it is clearly dominant (and, as shown in Figure 3, matches the results from Keylock *et al*. (2013) closely). Thus, as H increases and we see more extreme cases of velocity-intermittency, the dominant behaviour is that of the relatively slow but relatively turbulent contributions. The exceptions to this are the two positions at $z = 0.06$ m closest to the dune crest. At $x = 0.27$ m, there is also a positive contribution for Q4, while at $x = 0.18$ m Q1 is the dominant positive slope (squares in Figure 3). The results for flow over a mobile bedform exhibited an enhanced contribution in Q4 relative to those for the outer part of a boundary layer (Figure 1). Using the bed elevation data, Keylock *et al*. (2013) linked this to times when the probe was located in a wake region downstream of turbulence production by shear.

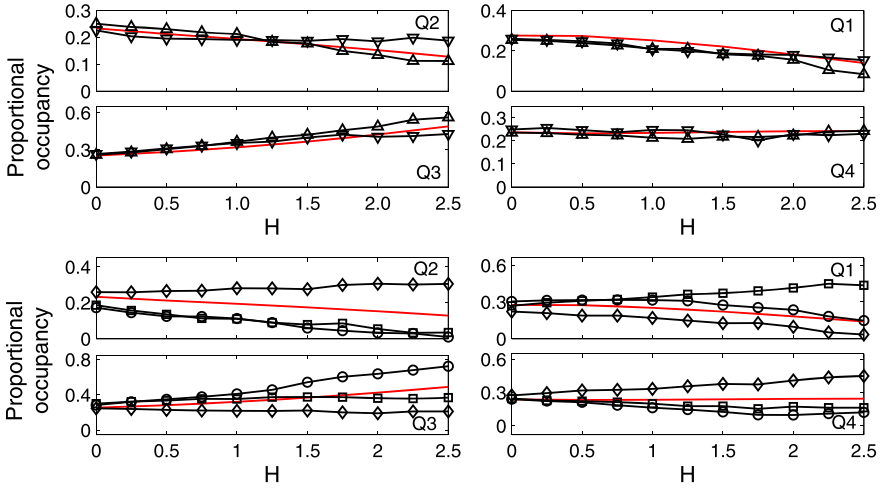

Figure 3. The proportional occupancy in each quadrant as a function of hole size, H. Results from Keylock *et al*. (2013) are shown as a solid red line. The upper plot shows data from ($x = 0.69$ m, $y = 0.06$ m) as downward triangles and ($x = 0.75$ m, $y = 0.06$ m) as upward triangles. The lower plot shows data from ($x = 0.69$ m, $y = 0.09$ m) as circles, ($x = 0.18$ m, $y = 0.06$ m) as squares and ($x = 0.36$ m, $y = 0.03$ m) as diamonds. These locations are highlighted in Figure 2 using labels (a)–(e), respectively.

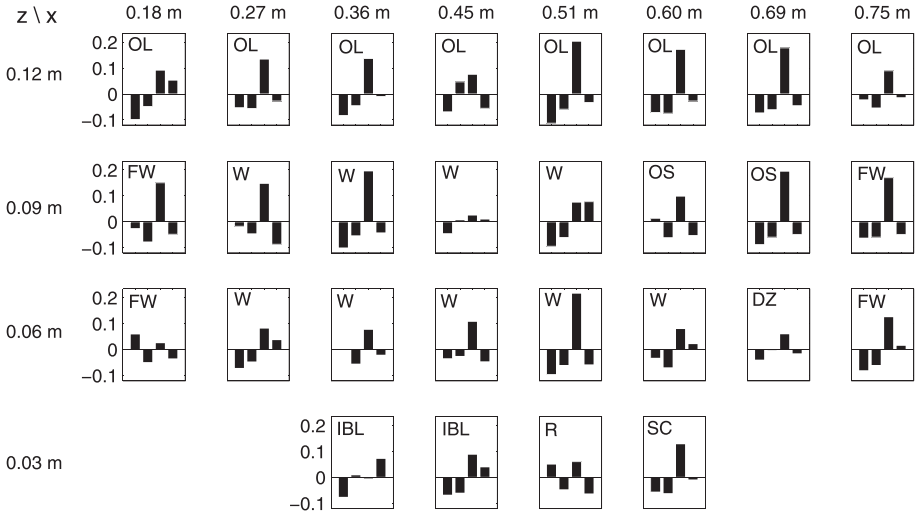

Figure 4. The slopes for the proportion of time that a quadrant is occupied against H for all 28 sites in the database from Venditti and Bennett (2000). The sampling locations are indicated in terms of x and z and each plot contains values for the slope for each quadrant, with Q1 on the left through to Q4 on the right. In addition, the labels used by Venditti and Bennett (2000) to describe the flow in each location are included: OL = outer layer; FW = far wake; W = wake; OS = over separation cell; DZ = dead zone; IBL = Internal boundary layer; R = reattachment.

The position of the ($x = 0.27$ m, $z = 0.06$ m) site suggests that it too is sampling these processes and the small positive slope in Q4 is consistent with the slope of the grey lines in Figure 1 for the wake data. Given that in Figure 1 it is the wake data that exhibit an overall dominance in Q1 at large H, our results from ($x = 0.18$ m, $z = 0.06$ m) are also readily interpretable.

Thus, at $z = 0.06$ m, and based on the velocity-intermittency characteristics shown in Figure 1, most sites are dominated by a bedform flow type or outer layer type, with some evidence for wake-like tendencies. The two sites closest to the crest seem to be dominated by wake processes. When we average over these eight datasets, we obtain the results seen in Figure 5(a), which match very closely those obtained by Keylock *et al.* (2013) seen in Figure 5(b). Hence, despite different flume facilities, flow conditions, time series durations and acquisition frequencies, and bedforms (prescribed geometry versus naturally evolved shape), and despite a change in the frame of reference from a study at fixed points over an immobile bed to one where the ADV samples various positions as bedforms are advected past, there is a remarkable agreement in the observed velocity-intermittency characteristics. This provides further support that the flow classification scheme recently proposed by Keylock *et al.* (2012c) is a robust, novel tool for environmental fluid mechanics, hydraulic and geomorphic research.

The primary difference between Figure 5(a) and 5(b) concerns the relative magnitudes of the negative slopes for Q1 and Q2. Keylock *et al.* (2013) found that Q1 was the larger negative slope, while averaging across $z = 0.06$ m shows that Q2 is greater. However, note that over the majority of positions in Figure 4, the same pattern as seen in Figure 5(b) is observed, meaning that the difference is an artefact of the averaging process. Hence methodological differences explain the small variation between Figure 5(a) and 5(b). Averaging across eight discrete positions does not weight locations in the same way as monitoring a single position as bedforms are advected past. In addition, the mean height of the probe in the results reported by Keylock *et al.* (2013) corresponded closely to $z = 0.06$ m, but departures towards conditions seen in Figure 4 at $z = 0.09$ m would place more of an emphasis on Q1.

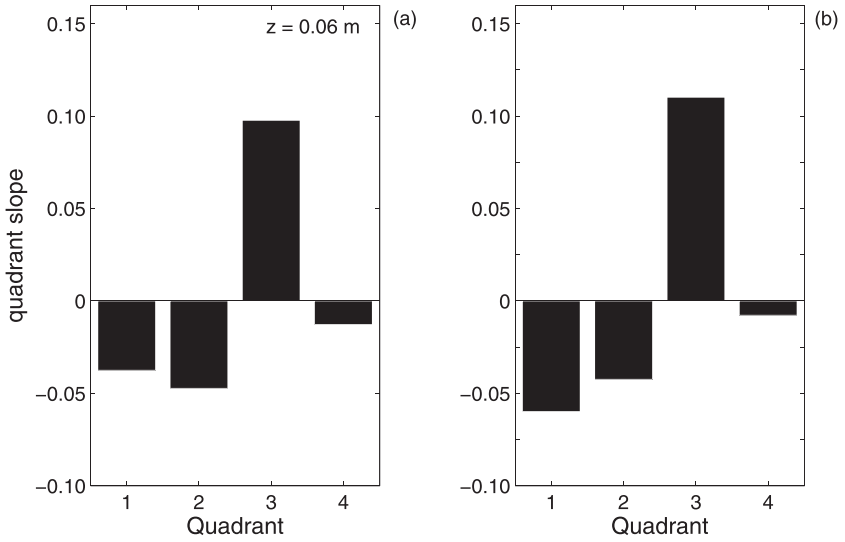

Figure 5. Slopes for the proportion of time that a quadrant is occupied against H. The results in panel (a) are averaged over the eight sites with $z = 0.06$ m. The results in (b) are those for the data taken over a mobile bedform (Keylock *et al.*, 2013).

Characteristics of the flow away from boundaries

Included in Figure 4 are the classification labels given to each data series by Venditti and Bennett (2000) based on an examination of the Reynolds stress, turbulent kinetic energy, boundary layer correlation, turbulence production and eddy viscosity (their Figure 5). Towards the free surface, the data from Venditti and Bennett (2000) are classified as 'OL' or outer layer. Figure 1 shows that the velocity-intermittency of an outer layer exhibits a positive slope in Q3, negative slopes in Q1 and Q4, with approximately neutral response in Q2. In contrast, Figure 1 shows that the bedform flow type data from Keylock *et al*. (2013) exhibits a strong, positive slope in Q3, with negative slopes in Q2 and Q1 and a more neutral response in Q4. An examination of Figure 4 shows that it is this latter situation that is more common at the positions classified as 'OL' by Venditti and Bennett (2000). Furthermore, in Figure 4, none of the data with a large Q3 contribution have their smallest negative response in Q2, which one would expect for the outer-layer velocity-intermittency structure from Figure 1. Hence, from the perspective of the velocity-intermittency structure, the outer layer seen here is not a classical outer part of a boundary layer. This indicates a difference in classification based on velocity intermittency and using more conventional variables and, as a consequence, we replace the 'OL' designation with the 'bedform flow (BF)' type.

The difference arises because the flow over bedforms inherits characteristics of macroturbulence generated by processes associated with shear and flow separation at and over the dune crest (Shvidchenko and Pender, 2001), the velocity-intermittency structure at $z = 0.12$ m exhibits behaviour seen closer to the bed by Keylock *et al*. (2013) in regions classified as 'wake' locations by Venditti and Bennett (2000). Because flow structures generated at the dune crest and in the lower part of the domain eventually fill much of the flow domain, for large H and when $u' < 0$, large-scale structures with significant intermittency arise. This explains the excessively high Q3 contribution found in this study relative to a classical outer layer (Figure 1). However, the positive slope in Q2 means that regions of low intermittency also persist, which implies a lack of complete mixing between the generated flow structures and the 'background' turbulence flow field. To understand how this difference will affect mixing relative to a boundary layer requires a comparative study of Lagrangian behaviour for the two cases. This is complicated by the fact that standard closure schemes in eddy-resolving simulation methods assume, following Kolmogorov (1941), that intermittency and velocity are independent (see Keylock *et al*., 2012a, for a review of applications of these methods in geomorphology). This implies that complex experiments or a direct numerical simulation are required to understand this result further.

Figure 5 shows that results similar to those from Keylock *et al*. (2013) can be obtained from the data of Venditti and Bennett (2000) by averaging over the positions at $z = 0.06$ m, a height that approximately corresponds to the mean height in the former study. However, it is important to note that Figures 3 and 4 show that time series from given positions also reveal the correct characteristics. Hence this agreement is not merely the consequence of an averaging over sites; it is the real behaviour seen at a particular spatial locations too.

Despite the results seen in Figure 5, it remains a possibility that there is a difference between the two datasets because, although the proportional occupancy of quadrants as a function of H is similar, one of these datasets contains preferentially high $|u_1'|$ and low $|\alpha_1'|$ values in a particular quadrant, while the other concentrates in regions of low $|u_1'|$ and high $|\alpha_1'|$. Figure 6 shows that there is no evidence for such a difference in these

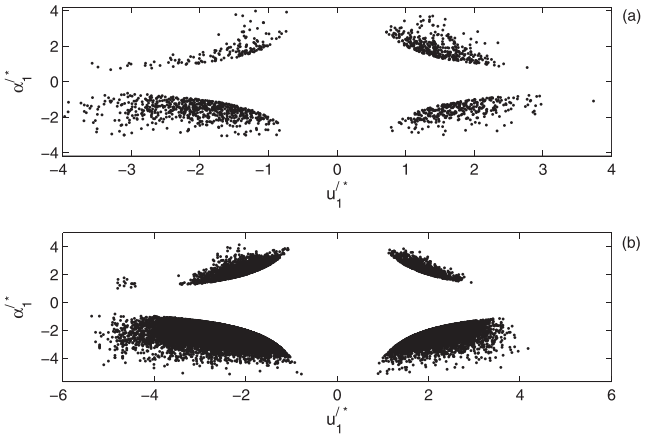

Figure 6. Velocity-intermittency plots for the data exceeding $H = 2$ at a height of $z = 0.06$ m (a) and for an exceedance of $H = 4$ for the data for flow over a mobile bedform (b).

data. The upper panel combines results for the eight positions at $z = 0.06$ m, also used in Figure 5, while the lower panel is for the mobile bed case. Owing to the three orders of magnitude difference in the number of samples in these cases, different values of H were chosen for illustrative purposes. For the fixed dune case we choose $H = 2$ and, for a normal distribution, such a threshold would be exceeded on one variable 4.6% of the time. The threshold for the mobile bed case is $H = 4$, which corresponds to 6.3×10^{-3}%.

The bedform flow velocity-intermittency structure and conventional quadrants

As defined above, bedform flow has a velocity-intermittency structure that is similar to the black line in Figure 1 and we suggested above that the reason this is more prevalent than a velocity-intermittency structure with outer flow characteristics is because of the presence of large-scale structures with significant intermittency. To check this, we examined the u_1' and u_3' time series at ($x = 0.69$ m, $z = 0.09$ m). Results from this site are shown in Figure 3 and, based on Figure 4, it appears to be a representative example.

Figure 7 shows a visualization of a conventional quadrant analysis (Bogard and Tiederman, 1986) applied to these data using the tools in Keylock (2007) and with a choice of conventional hole size, $H_c = 1.5$ to ensure that the extreme events are analysed (the results are not sensitive to this choice for $H_c > 1$). A 40 s a subset of the record is extracted to enhance visualization of the relevant flow structures. The advantage of this type of plot is that the standard quadrant analysis is accompanied by a wavelet decomposition. Hence one can determine, qualitatively, which wavelet scales (ordinate of the upper two panels) contribute to a given event, based on the strength of the shading (here we have chosen to normalize over all scales but separately for the two velocity components). Panel (c) shows that the data are dominated by ejections (white) and sweeps (black), in agreement with boundary layer theory (Nakagawa and Nezu, 1977). Figure 7 also highlights that for u_1 and $t \geq 60$ s it is scales 6–8 that contribute the greatest to the threshold exceedances, although the sweeps at $t = 67$ s and $t = 72$ s have energy distributed relatively evenly across higher frequencies. For $t \sim 60$ s, scales 6–8 also dominate the behaviour of u_3. However, for $t > 60$ s, the relevant contributions from u_3 are generally at lower scales/higher frequencies,

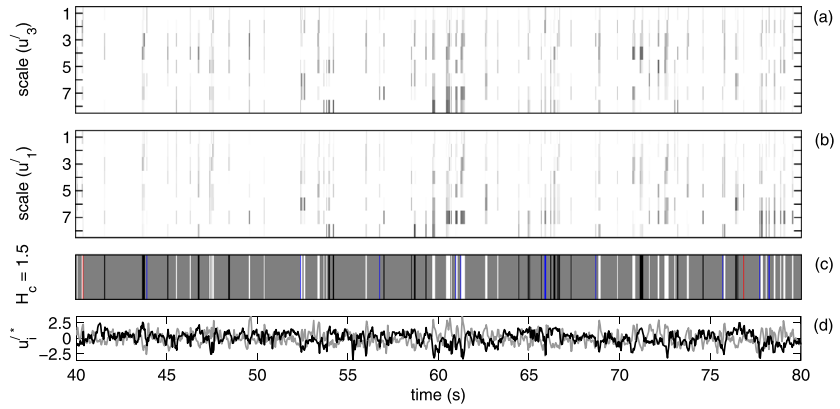

Figure 7. A wavelet and conventional quadrant decomposition of the velocity data at ($x = 0.69$ m, $z = 0.09$ m) with hole size $H_c = 1.5$. This location is position (c) in Figure 2. The bottom plot shows velocity time seriesfor u_1 (black) and u_3 (grey) with their means subtracted and normalized by their standard deviations; hence $u_1'*$ and $u_3'*$. Panel (c) indicates the times when the $H_c = 1.5$ criterion is exceeded by vertical lines: white = ejections, black = sweeps, outward interactions (red), inward interactions (blue). The thickness of each line indicates the length of time that the threshold is exceeded. The upper plots are wavelet decompositions of the flow field for each velocity component. Wavelet coefficients for the flow when $H_c < 1.5$ or that are opposite in nature to the sense of the flow event are ignored. The other coefficients are shaded proportional to their magnitude, with the shading normalized by the maximum absolute values across all scales, but separately for the two velocity components.

particularly at $t = 72$ s. For the first half of the record, no such patterns are as clearly discernible, owing in part to the increasing proportion of sweeps that occur at higher frequency. Thus, as expected from boundary layer theory, there is the anticipated dominant contribution from sweeps and ejections, with also some evidence for the different scales of variation observed in the outer part of a boundary layer. The dominance of inward interactions over outward interactions and of ejections over sweeps seen in Figure 7 does, however, suggest that when $u_1' < 0$ there is an enhanced propensity for energetic flow structures. This is borne out by the enhanced Q3 contributions in Figures 1, 3, 4 and 5 for the bed form flow type.

This supports the statement in the previous section that the reason the bedform flow type differs from a conventional outer layer in its velocity-intermittency structure is the relative enhancement of energetic contributions from Q3. This is made more explicit in Figure 8, where we examine the same period of data studied in Figure 7, but with quadrants formed in the manner described in this paper. The clear visual result is that the dominant quadrants are opposite in sense to those in Figure 7. Hence, when $u_1' < 0$, which clearly implies an ejection for $H > 1.5$, there is a highly intermittent Q3 contribution, while $u_1' > 0$ sweeps are preferentially in Q1, indicating lower turbulence levels than anticipated. Hence, from the perspective of flow structure identification methods based on the velocity gradient tensor, such as the 'Q-criterion' (Dubief and Delcayre, 2000; Chakraborty *et al.*, 2005), the sweep events in the bedform flow type may result in regions of high strain, but will make a limited contribution to vorticity and turbulence intensity.

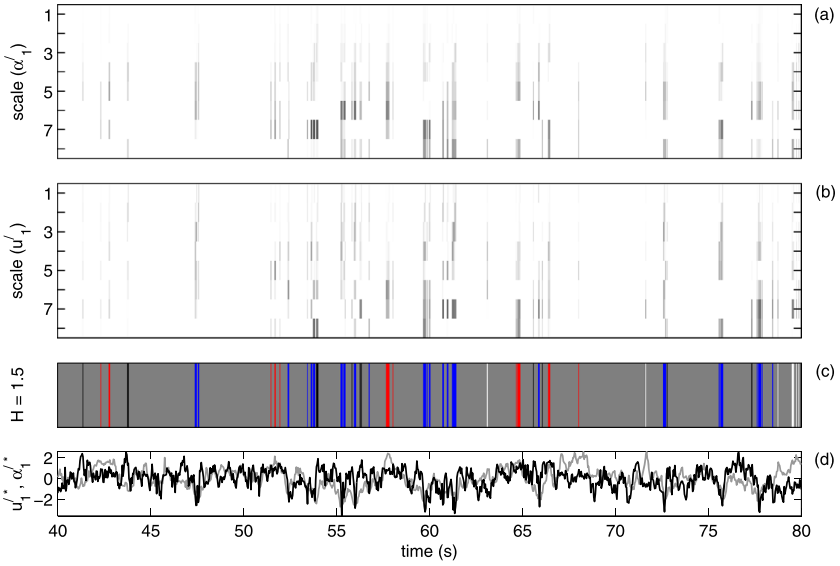

Figure 8. A wavelet and new quadrant decomposition of the velocity and Hölder exponent data at ($x = 0.69$ m, $z = 0.09$ m) with hole size $H_c = 1.5$. This location is position (c) in Figure 2. The bottom plot shows time series for u_1 (black) and α_1 (grey) with their means subtracted and normalized by their standard deviations; hence $u_1'*$ and $\alpha_1'*$. Panel (c) indicates the times when the $H = 1.5$ criterion is exceeded by vertical lines: Q2 (white), Q4 (black), Q1 (red) and Q3 (blue). The thickness of each line indicates the length of time that the threshold is exceeded. The upper plots are wavelet decompositions of the flow field for $u_1(t)$ and $\alpha_1(t)$. Wavelet coefficients for the flow when $H < 1.5$ or that are opposite in nature to the sense of the flow event are ignored. The other coefficients are shaded proportional to their magnitude, with the shading normalized by the maximum absolute values across all scales, but separately for the two variables.

Flow near the dune crest

Figure 1 shows that the far-wake generated by a cylinder placed vertically into the flow gives a positive slope in Q1, with a more limited positive response in Q4, a slight decline in Q3 and a significant decrease in Q2. The data at ($x = 0.18$ m, $z = 0.06$ m) are closest to the crest and are the only case of the 28 sites where Q1 gives the dominant positive response. The decay in Q2 is also consistent with the case of the cylinder wake. However, the behaviour in Q3 and Q4 is inverted. Whether this is significant or a consequence of the difference between a near-wake in the x–z plane and a far-wake in the x–y requires further investigation in another study.

While Venditti and Bennett (2000) categorized a large proportion of sites at $z = 0.06$ m as wake-like, based on their time-averaged statistics, in our case the majority of other sites at this elevation appear to have mixed wake and bedform flow characteristics. Given that it is from the study of velocity-intermittency characteristics at this mean elevation that we have been able to define the bedform flow class (Figure 1), it is not surprising that it influences wake characteristics for the flow in the lee of bedforms. The other site that appears to be dominated by wake-like phenomena is that at $x = 0.27$ m, where the positive response in Q4 is mixed with an outer layer-like or bedform flow-like positive response in Q3, meaning that the sign of the slope is dictated by α_1'.

Near-wall flow characteristics

At ($x \in \{0.36, 0.45\}$ m, $z = 0.03$ m), Venditti and Bennett (2000) classified the flow as 'IBL' or inner boundary layer. Figure 1 (blue and green solid lines) show the results for the velocity-intermittency structure of an inner boundary layer. A strong rise in Q4 is compensated by decreases in Q1 and Q3, with a neutral response in Q2. In a boundary layer, turbulence production is a consequence of positive Reynolds stresses, meaning that a standard quadrant analysis has an excess contribution of ejections and sweeps relative to inward and outward interactions (Nakagawa and Nezu, 1977). Close to the wall an ejection results in a compensatory inrush of turbulent fluid, generating a sweep that, because of its higher than average velocity and turbulent nature, results in a large contribution for Q4 from the perspective of our quadrant formulation. Note that ($x = 0.36$ m, $z = 0.03$ m) has the required Q4 response (Figure 4), although this does not apply for ($x = 0.45$ m, $z = 0.03$ m). This may be contrasted with the analysis for ($x = 0.69$ m, $z = 0.09$ m) in Figures 7 and 8, where the sweeps corresponded to Q1 rather than Q4. Thus our analysis is able to provide an insight into the nature of particular flow states that are deemed similar using conventional quadrant analysis.

Keylock *et al.* (2012c) also studied ADV time series obtained from a parallel-channel confluence experiment (Keylock *et al.*, 2014). The locations closest to the reattachment point exhibited slightly declining slopes in Q1 and Q2 with rises in Q3 and Q4, the pattern seen at ($x = 0.45$ m, $z = 0.03$ m). Although the three-dimensional nature of parallel-channel confluence flow means that the nature of reattachment is not a perfect analogue for a more two-dimensional bedform flow field, the similarity suggests that the velocity-intermittency results place reattachment slightly upstream of Venditti and Bennett (2000). This is not a contradiction because our method places emphasis on the extreme states, and the location of reattachment in a flow subject to an adverse pressure gradient fluctuates by more than ± 1 height of the object inducing flow separation (Eaton and Johnston, 1980; Aider *et al.*, 2007). In addition, in the same way that median velocity and skin friction criteria do not always yield the same result for the reattachment position (Le *et al.*, 1997), we emphasize a different aspect of the reattachment process with our method, meaning that perfect congruence is not necessarily expected.

At ($x = 0.51$ m, $z = 0.03$ m), we see positive slopes in Q1 and Q3, with negative slopes in Q2 and Q4. The results for a far wake regime in Figure 1 have the appropriate Q1 and Q2 response but are approximately flat in Q3, and exhibit a rise in Q4. The outer layer results in Figure 1 have the appropriate behaviour in Q3 and Q4. Hence turbulence at this location has a hybrid structure not seen in our previous work, the nature of which is a function of α_1'. The velocity-intermittency structure is the same as the wake flow seen at ($x = 0.18$ m, $z = 0.06$ m) in terms of the sign of each quadrant, if not magnitude. Hence the wake structure downstream of reattachment differs in nature from that in a shear layer. However, with vorticity already generated upstream, the greater emphasis on Q3 is to be expected.

The final near-bed site, at ($x = 0.60$ m, $z = 0.06$ m), was classified as within a separation cell by Venditti and Bennett (2000). Note from Figure 2 that this location is further from the bed than the other sites at $z = 0.06$ m and the velocity-intermittency characteristics are seen to be similar to bedform flow.

Ergodic considerations

The data obtained by Singh *et al.* (2010) and Venditti and Bennett (2000) are time series. However, turbulence physics is based on spatial velocity gradients. Typically, when the turbulence intensity is low enough, Taylor's hypothesis can be used to change from time to space based on the mean velocity. However, our intensities are too high for this. Hence we use an integrated version of Taylor's hypothesis due to Kahalerras *et al.* (1998), which we have found to give good results for higher intensities (Keylock *et al.*, 2012b). The standard Taylor approximation is given by

$$\frac{\partial}{\partial t} = - < u_1 > \frac{\partial}{\partial x_1} \tag{4}$$

Rather than use the mean velocity, we use the average local velocity (at times g and $g+1$) to derive our (no longer uniformly sampled) spatial positions, $x_1(r)$:

$$x_1(r) = -\sum_{g=0}^{r-1} \frac{u_1(g) + u_1(g+1)}{2} \Delta t \tag{5}$$

where $1 \leq r \leq N$ and g is a dummy variable. Thus a time series of N values with a constant interval between each point given by Δt is converted into a spatial series of N points, where the interval between each $x_1(r)$ is no longer constant. However, using a resampling method, a uniform spatial interval for the spatial series can be produced. Focusing on the location examined in detail in Figure 7 ($x = 0.69$ m, $z = 0.09$ m), the original values for the slopes in each quadrant (Figure 3) were -0.088, -0.059, 0.196 and -0.049, for Q1, Q2, Q3 and Q4, respectively. Following a recalculation of the Hölder exponents for the velocity series transformed into a spatial transect, the new slope values were -0.089, -0.056, 0.206 and -0.062. Thus, while the detail varies slightly as a consequence of the ergodic change, the changes are minor, indicating robustness of the method and the results.

As noted above, Venditti and Bennett (2000) classified their flow field based on the spatial location of the points and the observed behaviour of the turbulence intensities, Reynolds

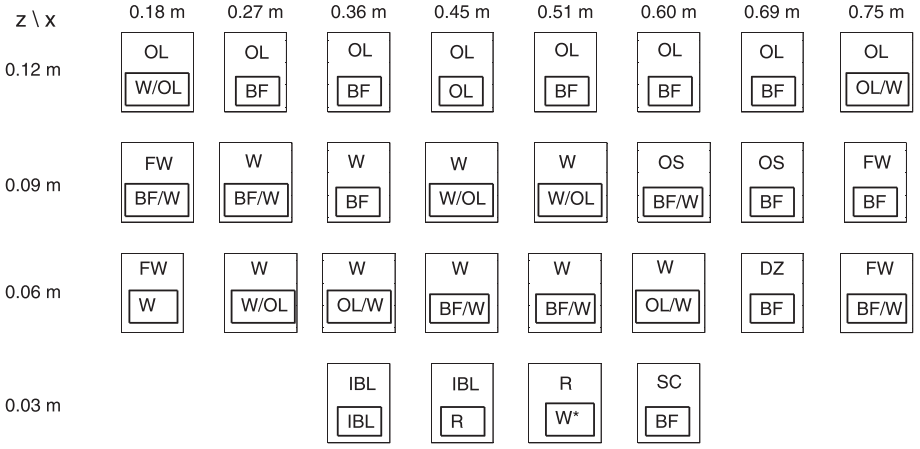

Figure 9. A comparison of the classification of dune flow data by Venditti and Bennett (2000) (upper values and Figure 4) and that found using the velocity-intermittency results in this study (in the lower box). For the original values: OL = outer layer; FW = far wake; W = wake; OS = over separation cell; DZ = dead zone; IBL = internal boundary layer; R = reattachment. In addition, from this study: BF = bedform flow, the asterisk discriminates between two types of wake and various sites are allocated mixed characteristics.

stresses etc. Figure 9 compares our classification to theirs based simply on the velocity-intermittency structure. Hence it summarizes most of the discussion presented in the previous section. If one considers the use of 'OL' for outer layer by Venditti and Bennett (2000) to be synonymous with our bedform flow 'BF' category, the agreement is very good. The distinction between these cases is based on the velocity-intermittency behaviour seen in Figure 1, which was a form of analysis not adopted in the earlier work. This excepted, the primary differences in the classification of the flow environment are that we locate reattachment one site upstream of Venditti and Bennett (2000) and find that most locations at $z = 0.06$ m (except those closest to the crest) have mixed wake and bedform flow characteristics as opposed to being allocated wake-like characteristics solely. Because our velocity-intermittency method works with $u_1'*$, differences in the variance between locations are normalized out. Furthermore, with no use of u_3', Reynolds stresses are inaccessible (and if one assumes that these correlate closely to u_1', then our normalization also removes this dependence). Hence velocity-intermittency as formulated here is virtually independent of conventional flow parameters used to infer flow structure, yet still contains requisite information of the flow characteristics, as Figure 9 illustrates. However, what our results emphasize, in contrast to the analysis undertaken by Venditti and Bennett (2000), is the role of individual, boundary-generated macroturbulent structures (Shvidchenko and Pender, 2001). Their effect is averaged out in a conventional analysis, but influences the velocity-intermittency structure and, consequently, the nature of the generated wakes. As a result, by comparing Figure 4 to Figure 1, we see that the bedform flow type dominates the flow field relative to the velocity-intermittency behaviour of wakes and outer layer flows.

Conclusion

This study has shown a remarkable level of agreement in the turbulence characteristics of two datasets for flow over bedforms despite the differences in bedform type, boundary conditions and experimental methods. Not only does this provide more evidence that the new turbulence classification of Keylock *et al.* (2012c) is robust, but it is also in agreement with a comparison between flow over dunes in the laboratory and the field using more conventional analysis methods (Venditti and Bauer, 2005). Classical analysis makes use of Reynolds stresses and turbulence intensities, i.e. terms based on the velocity variance–covariance matrix. Consequently, with such methods, it is simple to detect regions of turbulence production. Because our approach normalizes by the standard deviation of $u_1(t)$, that we can still define similar locations as having wake, reattachment, and inner or outer layer characteristics indicates the crucial role of the coupling between velocity and intermittency in anisotropic and non-homogeneous turbulent flows. However, our approach complements more conventional analyses based on mean properties by highlighting the role of flow structures on the turbulence characteristics. The results are also robust to a change from time series to spatial series using a modified form of Taylor's hypothesis.

As a consequence, given a set of time series, $u_1(t)$, derived in a complex environment, and with reference to the results obtained here and by Keylock *et al.* (2012c, 2013), it is possible to effectively assign each time series to a relevant flow type, e.g. 'the flow is "jet-like" in region *A*, while it resembles a wake in region *B*'. This method for turbulence flow classification is not only useful for highlighting to the researcher regions with different turbulence characteristics, but it also enables single-point measurements in the field or laboratory to be related to topological turbulence characteristics elucidated in the laboratory or numerically using the techniques discussed in the Introduction (Chakraborty *et al.*, 2005). The importance of coherent flow structures for fluvial processes is well established (see Venditti *et al.*, 2013, for a number of recent papers in this area). Hence this work permits a simpler comparison of the properties of such structures between field/laboratory and laboratory/modelling work.

Our study of velocity-intermittency coupling also opens up the possibility of deriving turbulence closures that are designed specifically for complex environmental flows. That is, rather than basing our modelling studies of flow near complex, geomorphic boundaries on closures that draw on classical understandings of turbulence to parametrize subfilter scale processes, this work establishes the potential to incorporate the observed velocity-intermittency coupling into energy dissipation equations. The more accurate near-wall modelling that would result would improve our ability to model flow resistance, pollutant dispersal and sediment transport. Our method is also likely to prove useful for developing new

sediment flux formulations. This is because impulse-based methods for sediment transport (Diplas *et al.*, 2008; Diplas and Dancy, 2013) require knowledge of the integrated force history. In the absence of local, near-wall time series, the time period for integration is not readily discernible from variables such as the Reynolds stress, but is much more so from the coupling between velocity and the Hölder exponents.

The technique used here is a generic method, applicable to any turbulent flow (and, indeed, any time series that exhibits considerable local fluctuations such as financial transaction data and sediment flux data). We believe it has significant potential in environmental fluid mechanics, where the complexity of boundary conditions means that classical ideas about the behaviour of turbulence do not necessarily hold. Such cases include, for example, flow through vegetated surfaces, which is a topic of current research.

Acknowledgements—AS and EFG acknowledge support by NCED (award EAR-0120914) and by NSF grants EAR-0824084 and EAR-0835789. CK acknowledges support for work developing signal-processing techniques as part of NERC award NE/F00415X/1. JV acknowledges support from an NSERC Discovery Grant and the Canadian Foundation for Innovation.

References

Aider JL, Danet A, Lesieur M. 2007. Large-eddy simulation applied to study the influence of upstream conditions on the time-dependent and averaged characteristics of a backward-facing step flow. *Journal of Turbulence* **8**: 1–30.

Best J. 2005. The fluid dynamics of river dunes: a review and some future research directions. *Journal of Geophysical Research* **110**: F04S02, doi: 10.1029/2004JF000218

Biron P, Roy A, Best JL. 1995. A scheme for resampling, filtering, and subsampling unevenly spaced laser Doppler anemometer data. *Mathematical Geology* **27**: 731–748.

Bogard DG, Tiederman WG. 1986. Burst detection with single-point velocity measurements. *Journal of Fluid Mechanics* **162**: 389–413.

Butler JB, Lane SN, Chandler JH. 2001. Characterization of the structure of river-bed gravels using two-dimensional fractal analysis. *Mathematical Geology* **33**: 301–330.

Chakraborty P, Balachandar S, Adrian RJ. 2005. On the relationships between local vortex identification schemes. *Journal of Fluid Mechanics* **535**:189–214.

Chang WY, Constantinescu G, Tsai WF, Lien HC. 2011. Coherent structure dynamics and sediment erosion mechanisms around an in-stream rectangular cylinder at low and moderate angles of attack. *Water Resources Research* **47**: W12532, doi: 10.1029/2011WR010586

Chapman CA, Walker IJ, Hesp PA, Bauer BO, Davidson-Arnott RGD. 2012. Turbulent Reynolds stress and quadrant event activity in wind flow over a coastal foredune. *Geomorphology* **151**: 1–12.

Dinehart R. 1992. Evolution of coarse gravel bed forms: field measurements at flood stage. *Water Resources Research* **28**: 2667–2689.

Diplas P, Dancey CL, Celik AO, Valyrakis M, Greer K, Akar T. 2008. The role of impulse on the initiation of particle movement under turbulent flow conditions. *Science* **322**: 717–720.

Diplas P, Dancy CL. 2013. Coherent flow structures, initiation of motion, sediment transport and morphological feedbacks in rivers. In Coherent Flow Structures at the Earth's Surface, Venditti JG, Best JL, Church M, Hardy RJ (eds). Wiley-Blackwell: Chichester; 289–307.

Dowker M, Ohkitani K. 2012. Intermittency and local Reynolds number in Navier–Stokes turbulence: a cross-over scale in the Caffarelli–Kohn–Nirenberg integral. *Physics of Fluids* **24**: 115112, doi: 10.1063/1.4767728

Dubief Y, Delcayre F. 2000. On coherent-vortex identification in turbulence. *Journal of Turbulence* **1**: 1–22.

Eaton JK, Johnston JP. 1980. Turbulent flow re-attachment: an experimental study of the flow and structure behind a backward-facing step. Technical Report MD-39, Stanford University.

Fernandez R, Best J Lopez F. 2006. Mean flow, turbulence structure, and bed form superimposition across the ripple-dune transition. *Water Resources Research* **42**: W05406, doi: 10.1029/2005WR004330

Franklin EM, Charru F. 2011. Subaqueous barchan dunes in turbulent shear flow. Part 1. Dune motion. *Journal of Fluid Mechanics* **675**: 199–222.

Frisch U, Sulem P, Nelkin M. 1978. Simple dynamical model of intermittent fully developed turbulence. *Journal of Fluid Mechanics* **87**: 719–736.

Gagnon J, Lovejoy S, Schertzer D. 2003. Multifractal surfaces and terrestrial topography. *Europhysics Letters* **62**: 801–807.

Haller G. 2001. Distinguished material surfaces and coherent structures in three-dimensional fluid flows. *Physica D* **149**: 248–277.

Hardy R, Lane S, Ferguson R, Parsons D. 2007. Emergence of coherent flow structures over a gravel surface: A numerical experiment. *Water Resources Research* **43**: W03422, doi: 10.1029/2006WR004936

Hardy RJ, Best JL, Parsons DR, Keevil GM. 2011. On determining the geometric and kinematic characteristics of coherent flow structures over a gravel bed: a new approach using combined PLIF-PIV. *Earth Surface Processes and Landforms* **36**: 279–284.

Hurst H. 1951. Long-term storage capacity of reservoirs. *Transactions of the American Society of Civil Engineers* **116**: 770–799.

Kahalerras H, Malécot Y, Gagne Y, Castaing B. 1998. Intermittency and Reynolds number. *Physics of Fluids* **10**: 910–921.

Keylock CJ. 2007. The visualisation of turbulence data using a wavelet-based method. *Earth Surface Processes and Landforms* **32**: 637–647.

Keylock CJ. 2008. A criterion for delimiting active periods within turbulent flows. *Geophysical Research Letters* **35**: L11804, doi: 10.1029/2008GL033858

Keylock CJ. 2009. Evaluating the dimensionality and significance of active periods in turbulent environmental flows defined using Lipshitz/Hölder regularity. *Environmental Fluid Mechanics* **9**: 509–523.

Keylock CJ. 2010. Characterizing the structure of nonlinear systems using gradual wavelet reconstruction. *Nonlinear Processes in Geophysics* **17**: 615–632.

Keylock CJ, Constantinescu G, Hardy R. 2012a. The application of computational fluid dynamics to natural river channels: eddy resolving versus mean approaches. *Geomorphology* **179**: 1–20.

Keylock CJ, Nishimura K, Nemoto M, Ito Y. 2012b. The flow structure in the wake of a fractal fence and the absence of an 'inertial regime'. *Environmental Fluid Mechanics* **12**: 227–250.

Keylock CJ, Nishimura K, Peinke J. 2012c. A classification scheme for turbulence based on the velocity-intermittency structure with an application to near-wall flow and with implications for bedload transport. *Journal of Geophysical Research* **117**: F01037, doi: 10.1029/2011JF002127

Keylock CJ, Singh A, Foufoula-Georgiou E. 2013. The influence of bedforms on the velocity-intermittency structure of turbulent flow over a gravel bed. *Geophysical Research Letters* **40**: 1–5.

Keylock CJ, Lane SN, Richards KS. 2014. Quadrant/octant sequencing and the role of coherent structures in bed load sediment entrainment. *Journal of Geophysical Research* **119**: 264–286.

Klinkenberg B, Goodchild MF. 1992. The fractal properties of topography: a comparison of methods. *Earth Surface Processes and Landforms* **17**: 217–234.

Kolmogorov AN. 1941. The local structure of turbulence in incompressible viscous fluid for very large Reynolds numbers. *Doklady Akademii Nauk SSSR* **30**: 299–303.

Kolmogorov AN. 1962. A refinement of previous hypotheses concerning the local structure of turbulence in a viscous, incompressible fluid at high Reynolds number. *Journal of Fluid Mechanics* **13**: 82–85.

Kolwankar KM, Lévy Véhel J. 2002. A time domain characterisation of the fine local regularity of functions. *Journal of Fourier Analysis and Applications* **8**: 319–334.

Le H, Moin P, Kim J. 1997. Direct numerical simulation of turbulent flow over a backward-facing step. *Journal of Fluid Mechanics* **330**: 349–374.

Lelouvetel J, Bigillon F, Doppler D, Vinkovic I, Champagne JY. 2009. Experimental investigation of ejections and sweeps involved in particle suspension. *Water Resources Research* **45**: W02416, doi: 10.1029/2007WR006520

Lu SS, Willmarth WW. 1973. Measurements of the structure of the Reynolds stress in a turbulent boundary layer. *Journal of Fluid Mechanics* **60**: 481–511.

Mazzi B, Vassilicos JC. 2004. Fractal-generated turbulence. *Journal of Fluid Mechanics* **502**: 65–87.

Meneveau C, Sreenivasan K. 1991. The multifractal nature of turbulent energy-dissipation. *Journal of Fluid Mechanics* **224**: 429–484.

Muzy JF, Bacry E, Arnéodo A. 1991. Wavelets and multifractal formalism for singular signals: application to turbulence data. *Physical Review Letters* **67**: 3515–3518.

Nakagawa H, Nezu I. 1977. Prediction of the contributions to the Reynolds stress from bursting events in open channel flows. *Journal of Fluid Mechanics* **80**: 99–128.

Nelson JM, Shreve RL, McLean SR, Drake TG. 1995. Role of near-bed turbulence structure in bed load transport and bed form mechanics. *Water Resources Research* **31**: 2071–2086.

Omidyeganeh M, Piomelli U. 2013a. Large-eddy simulation of three-dimensional dunes in a steady, unidirectional flow. Part 1. Turbulence statistics. *Journal of Fluid Mechanics* **721**: 454–483.

Omidyeganeh M, Piomelli U. 2013b. Large-eddy simulation of three-dimensional dunes in a steady, unidirectional flow. Part 2. Flow structures. *Journal of Fluid Mechanics* **734**: 509–534.

Posadas AND, Gimenez D, Quiroz R, Protz R. 2003. Multifractal characterization of soil pore systems. *Soil Science Society of America Journal* **67**: 1361–1369.

Renner C, Peinke J, Friedrich R. 2001. Experimental indications for Markov properties of small-scale turbulence. *Journal of Fluid Mechanics* **433**: 383–409.

Roy A, Buffin-Bélanger T, Lamarre H, Kirkbride A. 2004. Size, shape and dynamics of large-scale turbulent flow structures in a gravel-bed river. *Journal of Fluid Mechanics* **500**: 1–27.

Schertzer D, Lovejoy S. 1987. Physical modeling and analysis of rain and clouds by anisotrpic scaling of multiplicative processes. *Journal of Geophysical Research* **92**: 9693–9714.

Seuret S, Lévy Véhel J. 2003. A time domain characterization of 2-microlocal spaces. *Journal of Fourier Analysis and Applications* **9**: 473–495.

Shvidchenko A, Pender G. 2001. Macroturbulent structure of open-channel flow over gravel beds. *Water Resources Research* **37**: 709–719.

Singh A, Fienberg K, Jerolmack D, Marr J, Foufoula-Georgiou E. 2009. Experimental evidence for statistical scaling and intermittency in sediment transport rates. *Journal of Geophysical Research* **114**: F01025, doi: 10.1029/2007JF000963

Singh A, Porté-Agel F, Foufoula-Georgiou E. 2010. On the influence of gravel bed dynamics on velocity power spectra. *Water Resources Research* **46**: W04509, doi: 10.1029/2009WR008190

Singh A, Lanzoni S,Wilcock P, Foufoula-Georgiou E. 2011. Multiscale statistical characterization of migrating bed forms in gravel and sand bed rivers. *Water Resources Research* **47**: W12526, doi: 10.1029/2010WR010122

Stresing R, Peinke J, Seoud S, Vassilicos J. 2010. Defining a new class of turbulent flows. *Physical Review Letters* **104**: 194501, doi: 10.1103/PhysRevLett.104.194501

Venditti JG, Bennett SJ. 2000. Spectral analysis of turbulent flow and suspended sediment transport over fixed dunes. *Journal of Geophysical Research* **105**: 22035–22047.

Venditti JG, Bauer BO. 2005. Turbulent flow over a dune: Green River, Colorado. *Earth Surface Processes and Landforms* **30**: 289–304.

Venditti JG, Best JL, Church M, Hardy RJ (eds). 2013. Coherent Flow Structures at the Earth's Surface. Wiley-Blackwell: Chichester; 289–307.

Venugopal V, Roux S, Foufoula-Georgiou E, Arneodo A. 2006. Revisiting multifractality of high-resolution temporal rainfall using a wavelet-based formalism. *Water Resources Research* **42**: W06D14, doi: 10.1029/2005WR004489

Walker IJ, Nickling WG. 2002. Dynamics of secondary airflow and sediment transport over and in the lee of transverse dunes. *Progress in Physical Geography* **26**: 47–75.

